THE JOURNAL OF PHYSICAL CHEMISTRY C

pubs.acs.org/JPCC Article

Electronic and Transport Properties in Defective MoS_2: Impact of Sulfur Vacancies

Sai Manoj Gali,* Anton Pershin, Aurélien Lherbier, Jean-Christophe Charlier, and David Beljonne*

Cite This: J. Phys. Chem. C 2020, 124, 15076−15084 Read Online

ACCESS | Metrics & More | Article Recommendations | Supporting Information

ABSTRACT: Crystal impurities, such as atomic vacancies, are known to modulate the charge transport characteristics of two-dimensional (2D) materials. Here, we apply a first-principles-enriched tight-binding modelling approach to assess the influence of sulfur vacancies on the electronic structure and quantum transport characteristics of MoS_2 monolayers. To this end, an sp^3d^5 orthogonal tight-binding (oTB) model of the pristine and defective MoS_2 monolayer is mapped with electronic structure calculations performed at the density functional theory level and subsequently used in the real-space Kubo−Greenwood (KG) scheme for charge transport simulations. The calculated charge carrier mobility is found to be sensitive to both the density and spatial arrangement of vacancies. Our oTB/KG simulations predict a drop of mobility by two orders of magnitude when the vacancy concentration is increased from 0.1 to 3%, in excellent agreement with experimental results. The simulation of realistic samples (including specific types of defects) pave a new route toward the accurate understanding and the possible prediction of 2D materials for nanoelectronic devices.

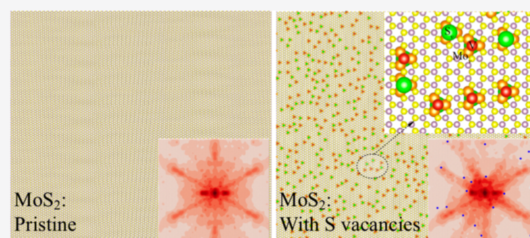

Downloaded via UNIV DE MONS on August 17, 2020 at 09:05:23 (UTC).
See https://pubs.acs.org/sharingguidelines for options on how to legitimately share published articles.

■ INTRODUCTION

The reduced dimensionality and symmetry of two-dimensional (2D) materials generate physical phenomena that are quite different from their three-dimensional (3D) counterparts.[1,2] The unique properties of graphene,[3,4] the archetype of 2D materials, have triggered a scientific fervor toward the development of several alternative 2D structures such as metal chalcogenides, metal−organic frameworks, metal oxides, and hydroxides,[5,6] with biological and/or optoelectronic applications.[7−9] Atomic monolayers of transition-metal dichalcogenides (TMDCs) such as MoS_2, $MoSe_2$, WS_2, and WSe_2 have rapidly emerged as a class of promising alternative 2D materials for their high carrier mobility (up to ≈100 $cm^2\ V^{-1}\ s^{-1}$), sizeable direct band gap (1−3 eV), and mechanical flexibility.[10] The most investigated 2D-TMDCs is the MoS_2 monolayer, both experimentally and theoretically, serving as a prototypical example for the other TMDCs and has been successfully used as the active layer in optoelectronic devices, electronic switches, and as photodetectors in solar cells.[11−13] Previous theoretical investigations have attempted to understand the intrinsic nature of charge transport in 2D TMDCs,[14,15] and seminal studies by Kaasbjerg *et al.* estimated the electron mobilities of the MoS_2 monolayer to be of the order of ≈400 $cm^2\ V^{-1}\ s^{-1}$ using semiclassical Boltzmann transport equation (scBTE).[16] However, the theoretical charge-carrier mobilities do not fare well with the experimental mobilities measured in field-effect transistor configurations because of the residual electron scattering at the semiconductor−dielectric interface dominated by the ubiquitous Coulomb impurities and the nonlinear dependence of free-carrier density of the charge carriers as a function of gate voltage.[17,18] Another source of residual scattering originates from chemical defects, such as grain boundaries, dislocations, and sulfur vacancies, which are commonly observed in MoS_2 samples obtained by chemical vapor deposition.[19−22] These, sometimes, appear jointly leading to the formation of vacancy complexes that have been evoked to explain the switching mechanism in memtransistors.[23] However, most common and important of these intrinsic defects are "sulfur" vacancies in the case of MoS_2 samples, with an estimated concentration of ≈3%.[24−26] These vacancies are reported to be thermodynamically stable[20,22] and largely affect the charge transport characteristics.[27,28] While controlled density of sulfur vacancies is desirable for modulating the catalytic activity of MoS_2,[29,30] the presence of sulfur vacancies, in itself, could be detrimental to the charge-carrier mobility. Some of us have investigated the impact of sulfur vacancies on charge-carrier mobilities by systematically engineering the experimental defect densities through the irradiation of 2D MoS_2 sheets with ion beams and by employing scBTE.[31] However, despite the good agreement with experimental data, theoretical charge carrier mobilities reported in ref 31 are obtained by including the impurity scattering mechanism in a phenomenological way and neglecting the actual variation of electronic structure of the

Received: May 11, 2020
Revised: June 17, 2020
Published: June 18, 2020

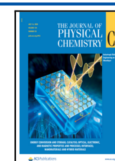

ACS Publications © 2020 American Chemical Society

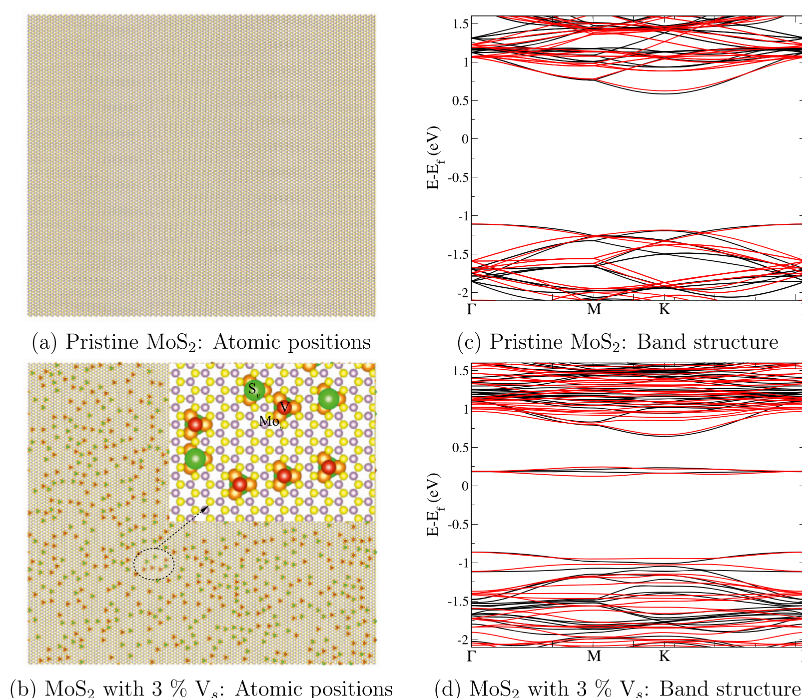

Figure 1. Atomic positions of MoS_2 with (a) top, left: no sulfur vacancies and (b) bottom, left: with 3% sulfur vacancies present on both sides of the monolayer. Sulfur vacancies (V_S) and the sulfur atoms (S_v) on the opposite side vacancy atoms are represented in red and green, respectively. Sulfur and molybdenum atoms are magnified to represent the distribution. Comparison of the band structure obtained with DFT (black curves) to that obtained using the oTB parameters (red curves) for (c) top, right: pristine MoS_2 and (d) bottom, right: MoS_2 with 3% sulfur vacancy.

material as a function of defect concentration. Although, the variations in the band structure and/or densities of states in defective systems/monolayers are tractable with first-principles calculations, these *ab initio* simulations become computationally expensive to treat large systems, which are essential to duplicate realistic experimental structures and/or to replicate structures with low-defect densities.

Tight-binding (TB) models offer an attractive alternative in efficiently treating the electronic structure of large systems. By employing the Kubo–Greenwood (KG) formalism, based on well-adjusted TB models, it is possible to predict the charge carrier mobilities of the MoS_2 monolayer, as a function of sulfur vacancies. The full-quantum real space order-N KG formalism has been successfully employed in the past to study the transport characteristics of graphene[32−34] by explicitly taking into account the changes in electronic structure of the material as well as the time and energy-dependent wave packet scattering in the presence of structural defects.[35−37] Also, the simulations can be performed on larger systems/super cells[38,39] containing few thousand to a million atoms, which is computationally prohibitive for the scBTE. Previous studies employed a nonorthogonal TB model involving 3d orbitals for transition metal and 3p orbitals for the chalcogen sulfur atom,[40] to estimate the electrical conductivities of MoS_2 and WS_2 monolayers as a function of sulfur vacancies (up to 1%).[41] However, the resulting electronic band structure of MoS_2 and WS_2 in their multilayer and monolayer forms show considerable discrepancies with those obtained using density functional theory (DFT). Alternatively, Zahid *et al.* developed a nonorthogonal sp^3d^5 TB model for pristine MoS_2 with a better match of the TB electronic band structure to that of the *ab initio* calculations.[42] Here, we report on the development of a simpler orthogonal sp^3d^5 tight-binding (oTB) model for MoS_2 monolayer that correctly reproduces the reference DFT electronic structure not only in its pristine form but also in the defective form containing a small concentration of sulfur vacancies. These oTB parameters are further incorporated into the KG simulation scheme estimating the band and field effect mobilities of the MoS_2 monolayer as a function of sulfur vacancy concentration. The estimated mobilities are compared with the previously reported experimental and theoretical electron mobilities obtained using the scBTE[31] and in excellent agreement. The effect of spatial arrangement of the sulfur vacancies at a fixed vacancy concentration on the estimated band mobilities is also discussed.

Computational Details. The orthogonal TB (oTB) model for the MoS_2 monolayer was developed by employing the band structure fitting strategy, wherein the electronic band structure obtained by plane-wave DFT is taken as the reference and is compared to that obtained by TB calculations. oTB parameters were subsequently derived by minimizing the error between the reference eigenvalues and those from the TB calculations, using

$$S(P) = \sum_{j} \sum_{k} \frac{[E^{\mathrm{TB}}_{(j,k)} - E^{\mathrm{DFT}}_{(j,k)}]^2}{{\sigma_{(j,k)}}^2} \quad (1)$$

where $E^{\mathrm{TB}}_{(j,k)}$ and $E^{\mathrm{DFT}}_{(j,k)}$ correspond to the eigenvalues of the jth band at the kth k-point, obtained using oTB model and DFT calculations, respectively, and ${\sigma_{(j,k)}}^2$ is the weight being equal for each data point. The numerical derivatives of the error from eq 1 with respect to each TB parameter were incorporated into the Broyden–Fletcher–Goldfarb–Shanno algorithm, accelerated by an efficient line search scheme. All TB calculations were performed using the TB_Sim code, which was earlier employed to investigate the charge transport characteristics in graphene layer as a function of structural defects[35,43] and correlated energetic disorder.[44] The TB_Sim code was

https://dx.doi.org/10.1021/acs.jpcc.0c04203
J. Phys. Chem. C 2020, 124, 15076−15084

appropriately modified to include the structure of the MoS_2 monolayer, in its pristine and defective (sulfur vacancies) forms. DFT calculations were carried out using Quantum−Espresso test suite[45] with PBE functional for a hexagonal unit cell (a = 3.1790 Å and c = 30.00 Å) and uniform Monkhorst−Pack mesh of 12 × 12 × 1 for pristine MoS_2 monolayer. Here, six bands, including two occupied and four unoccupied states, were considered to extract the oTB parameters. The oTB parameters for the MoS_2 monolayer in the presence of sulfur vacancies were computed using a 4 × 4 × 1 hexagonal super cell at the same level of theory, where the transfer integrals between sulfur vacancy and other surrounding atoms were set to zero, while its on-site energy was set to a very large value (30 eV) in order to remove spurious localized states from the energy window of interest. To refine the resulting band structure for the defected MoS_2, the interaction parameters of the three neighboring Mo and of the opposite S atoms were tuned, using the fitting procedure described above. The oTB parameters are reported in the Supporting Information, Table S1. It is to be noted that sulfur vacancy concentrations indicated as percentage in this work represent the fraction of sulfur atoms removed with respect to the total number of sulfur atoms present in the monolayer. The atomic positions of the pristine MoS_2 monolayer and for the monolayer with 3% sulfur vacancy concentration, along with the corresponding TB and DFT electronic band structures of a 4 × 4 supercell are presented in Figure 1. TB versus DFT band structure fit employed to derive the oTB parameters is reported in Figure S1. The pristine MoS_2 monolayer shows a direct DFT band gap of 1.63 eV at the K-point, in close quantitative agreement with the previous results.[46,47] Defective MoS_2 with 3% sulfur vacancy shows two additional/defect states very close to the conduction band edge and one defect state very close to the valence band edge, with a transition to the indirect band gap. The variation of sulfur vacancy concentration, however, changes the broadening of the defect state because of the interacting sulfur vacancies.[47,48] The band structure of the MoS_2 monolayer obtained from the oTB parameters is in good quantitative agreement with those obtained from DFT calculations, both in-terms of the electronic band gap as well as the band dispersion.

Subsequently, the oTB model was coupled to a real-space order-N KG simulation scheme[32−34,43,49,50] to extract the transport quantities of pristine and defective forms of the MoS_2 monolayer associated to the different transport regimes (ballistic, diffusive, and localized). The transport quantities, derived from the wave packet dynamics as a function of energy E, are characterized by the time-dependent diffusivity, $D(E,t)$, given by

$$D(E, t) = \frac{\Delta R^2(E, t)}{t} \tag{2}$$

where the mean quadratic spread of the wave packet, $\Delta R^2 = \Delta X^2 + \Delta Y^2$, along the directions X and/or Y is computed from the Hamiltonian and the position operator is $\hat{X}(E,t)$ as

$$\Delta X^2(E, t) = \frac{\mathrm{Tr}[\delta(E - \hat{H})|\hat{X}(t) - \hat{X}(0)|^2]}{\mathrm{Tr}[\delta(E - \hat{H})]} \tag{3}$$

where Tr is the trace over sp^3d^5 orbitals and $\mathrm{Tr}[\delta(E - \hat{H})]/S = \rho(E)$ is the total density of states (DOS) per unit surface area, S. Heisenberg representation $\hat{X}(t) = \hat{U}^\dagger(t)\hat{X}(0)\hat{U}(t)$ and $\hat{Y}(t) = \hat{U}^\dagger(t)\hat{Y}(0)\hat{U}(t)$ are used to express the position operators $\Delta\hat{X}^2(E,t)$ and $\Delta\hat{Y}^2(E,t)$, where $\hat{U}(t) = \prod_{n=0}^{N-1} \exp(i\hat{H}\Delta t/\hbar)$ is the time evolution operator and Δt is the time step computed with the Chebyshev polynomial expansion method.[49,50] Calculations were performed with eight initial random phases of the wave packet distributed on each orbital of the large 64 × 94 supercell of the pristine and defective MoS_2 monolayers. The system is 35.23 nm along the armchair direction (set to x axis) and 30.51 nm along the zigzag configuration (set to y axis), both long enough to avoid finite size effects as periodic boundary conditions are applied. Sulfur vacancies were created by removing sulfur atoms randomly or following a particular spatial distribution ("*vide infra*") in any case keeping a minimum cut-off distance of 7 Å between two sulfur vacancies and modulating the defect density between 0.1 and 3.0%. The time-dependent diffusivity coefficient ($D(E,t)$), is computed to extract the conductivity ($\sigma_{sc}(E_F,T)$) and mobility ($\mu_{KG}(E,T_F)$) in the semiclassical asymptotic limit (see ref 35 for details) as

$$\sigma_{sc}(E, 0\ \mathrm{K}) = \frac{1}{4}e^2\rho(E)D_{max}(E)$$

$$\sigma_{sc}(E_F, T) = \int_{-\infty}^{\infty} \mathrm{d}E' \frac{\partial f(E', E_F, T)}{\partial E'}\sigma_{sc}(E', 0\ \mathrm{K}) \tag{4}$$

$$\mu_{KG}(E_F, T) = \frac{\sigma_{sc}(E_F, T)}{en(E_F, T)} \tag{5}$$

where e is the elementary charge, E_F is the Fermi energy, $f(E',E_F,T)$ is the Fermi-Dirac distribution for a given (electronic) temperature T, which was set to room temperature of 300 K, $n(E_F,T)$ is the charge carrier density, and D_{max} is the diffusivity coefficient at the semiclassical asymptotic limit (i.e., $\lim_{t\to\infty} D[t] = D_{max}$). Indeed in the diffusive transport regime, the diffusivity saturates to a given value, while in the ballistic case, it continues to increase linearly with time.

■ RESULTS AND DISCUSSION

KG simulations were performed on the MoS_2 monolayer, in its pristine form and with sulfur vacancies, to extract the transport characteristics (σ_{sc} and μ_{KG}) in the semiclassical asymptotic limit. In the following sections, the impact of different spatial distributions of sulfur vacancies, created at a fixed vacancy concentration, on the charge carrier mobilities of the MoS_2 monolayer is discussed. Subsequently, the charge carrier mobilities of the MoS_2 monolayer in the presence of various concentrations of randomly distributed sulfur vacancies are discussed in conjunction with the available experimental data.

Sulfur Vacancies: Impact of Spatial Distribution. The density of sulfur vacancies can be controlled experimentally, by suitably tuning the experimental conditions such as time and duration of ion beam irradiation,[31] electron irradiation,[51] or by thermal annealing.[30] However, these sulfur vacancies can be present as isolated defects or as cluster of vacancies, which can be either on one side or on both the sides of the MoS_2 monolayer.[52−55] In order to elucidate the impact of different arrangements of sulfur vacancies, present either as isolated or as cluster of vacancies, on the electron mobility of the MoS_2 monolayer, we consider different vacancy arrangements at a fixed vacancy concentration of 1.5%. First, the charge transport characteristics of MoS_2 with sulfur vacancies (V_S) randomly distributed on both sides of the monolayer are compared to those where the random vacancies are created only on one side, which are hitherto referred to as rD_2 and rD_1, respectively.

https://dx.doi.org/10.1021/acs.jpcc.0c04203
J. Phys. Chem. C 2020, 124, 15076−15084

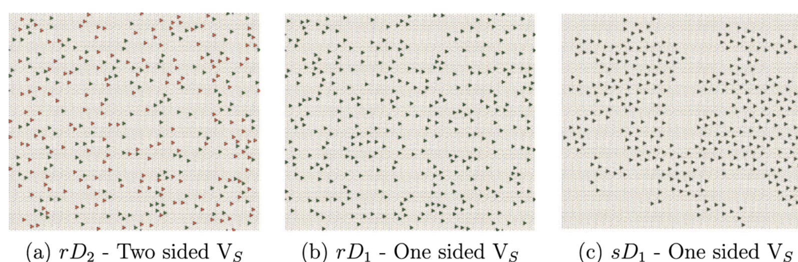

Figure 2. Atomic positions of MoS_2 with 1.5% sulfur vacancies, (a) left: random sulfur vacancies on both sides of the MoS_2 monolayer (rD_2), (b) middle: random sulfur vacancies on only one side of the MoS_2 monolayer (rD_1), (c) right: spatial distribution of sulfur vacancies on top side of the monolayer (sD_1). Sulphur vacancies (V_S) on one side of the monolayer are indicated by green and on the other side by red. Vacancy atoms are magnified to show the distribution.

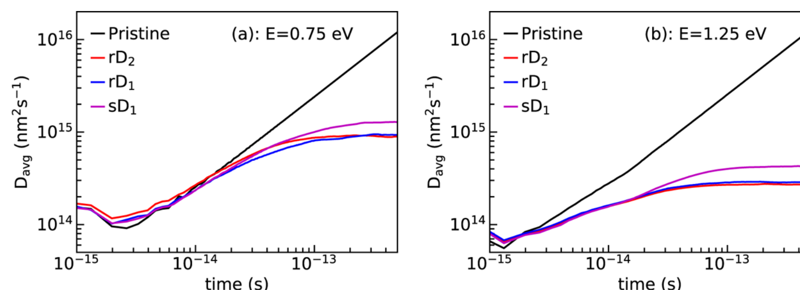

Figure 3. Diffusion coefficient of MoS_2, with 1.5% sulfur vacancies, obtained at different energies for the carriers (a) left: 0.75 eV in the conduction band and (b) right: 1.25 eV in the conduction band. Sulfur vacancies are arranged either randomly: on both sides of the monolayer (rD_2: red curves) and only one side (rD_1: blue curves) or with a spatial distribution of vacancies (sD_1: magenta curves). Black curves represent the pristine case, when no sulfur vacancies are present.

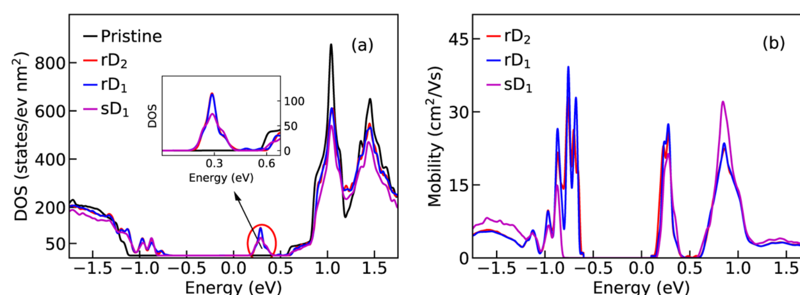

Figure 4. DOS and mobility of the MoS_2 monolayer, with 1.5% sulfur vacancies. Sulfur vacancies are arranged either randomly: on both sides of the monolayer (rD_2: red curves) and only one side (rD_1: blue curves) or with a spatial distribution of vacancies (sD_1: magenta curves). The mathematical divergence when $E \simeq 0$ is removed from the mobility plots for the sake of clarity.

Subsequently, spatial distribution of sulfur vacancies are created on one side of the monolayer, so as to contain well-separated cluster of defects that are distributed in space imposing an interaction potential between two sulfur vacancies with an equilibrium distance of 11 Å, hitherto referred to as sD_1. The charge transport characteristics of sD_1 are compared to those obtained using random distribution of sulfur vacancies, that is, rD_1 and rD_2. The spatial arrangements of the aforementioned sulfur vacancy types on the MoS_2 monolayer, following a nomenclature of xD_y, x representing random (r) or spatial (s) and y representing one side (1) or two sides (2), are presented in Figure 2.

The diffusion coefficients of the wave packet spread [$D(E,t)$ as defined in eq 2] for random sulfur vacancies present either on two sides (rD_2) or on one side of the monolayer (rD_1), along with the spatially distributed vacancies (sD_1) are presented in Figure 3, at conduction band energies (E) of 0.75 eV and 1.25 eV. $D(E,t)$ accounts for both the arm-chair and zig-zag directions of the pristine/defective MoS_2 monolayer. After roughly 5 femtoseconds (fs), a time corresponding to the onset of the spreading of the wavepacket over few atomic distances, the diffusion coefficient in pristine MoS_2 shows a ballistic regime, wherein the diffusion coefficient increases linearly with the diffusion time. In the presence of sulfur vacancies, D_t shows an initial ballistic transport followed by a plateau, indicating the semiclassical asymptotic limit (D_{max}). For random sulfur vacancies arranged either on one side or on both sides of the monolayer (rD_1 and rD_2), D_{max} remains the same at conduction band energies (E) of 0.75 eV and 1.25 eV. However, D_{max} is comparatively larger where sulfur vacancies are arranged spatially (sD_1). It follows that, at any given sulfur vacancy concentration, random sulfur vacancies present either on both sides or only on one side of the monolayer generates the same diffusion coefficient in the semiclassical asymptotic limit (D_{max}), whereas the presence of spatially correlated sulfur vacancies at the same vacancy concentration can induce a variation in the diffusion coefficient.

https://dx.doi.org/10.1021/acs.jpcc.0c04203
J. Phys. Chem. C 2020, 124, 15076−15084

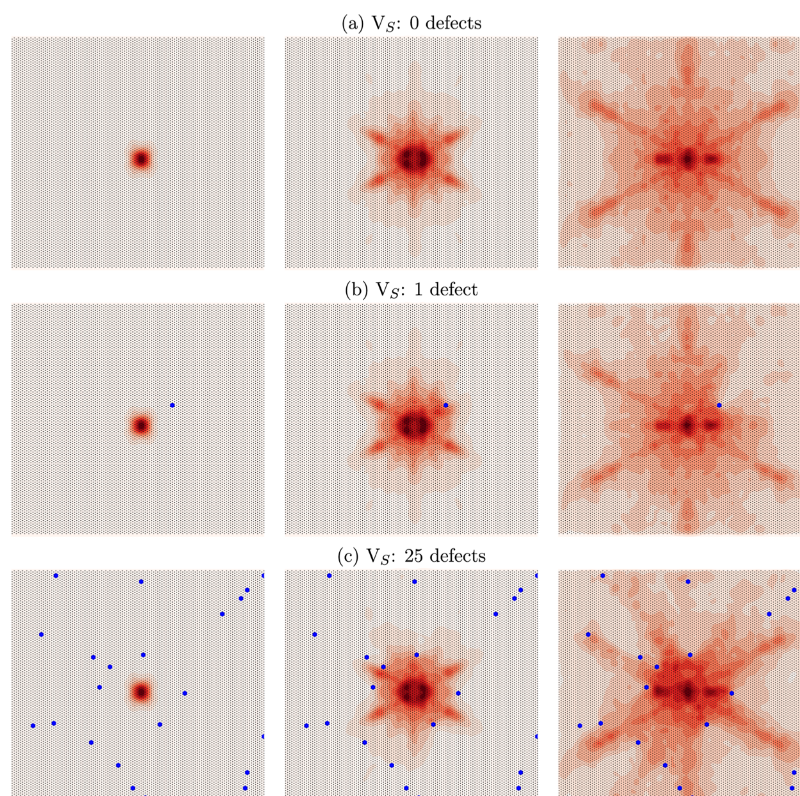

Figure 5. Time evolution of one EWF of the MoS_2 monolayer with (a) top: zero sulfur vacancies (pristine form), (b) middle: one sulfur vacancy, and (c) bottom: twenty-five random sulfur vacancies. The snapshots, from left to right, were extracted at simulations times of 5.85, 24.05, and 52.65 fs, respectively. V_S represents the number of sulfur vacancies.

The DOS and charge carrier mobilities (evaluated with KG simulation scheme, see eq 5) as a function of Fermi energy (E_F which can be modulated by a gate voltage) for random and spatial distribution of sulfur vacancies are presented in Figure 4. The DOS for the MoS_2 monolayer with random sulfur vacancies are identical when vacancies are present either on both sides or only on one side of the monolayer (rD_2 and rD_1), whereas when sulfur vacancies are spatially arranged (sD_1), the DOS shows small variations with respect to randomly arranged vacancies. In line with the band structure reported in Figure 1, the DOS of pristine MoS_2 exhibits a clear band gap of 1.63 eV, whereas in the defective case, additional peaks appear within this band gap (defect states) because of the presence of sulfur vacancies (see the inset of Figure 4a). These additional (defect) states, localized with a maximum at band energies of ≈0.3 eV also contribute to the band mobilities within the band gap, indicated by nonzero mobilities (μ) at $E \approx 0.3$ eV, as reported in Figure 4b. Further, while the charge carrier mobilities ($\mu_{KG}(E_F)$) are identical when random sulfur vacancies are present either on two sides or only on one side of the monolayer, $\mu_{KG}(E_F)$ are competitively larger when vacancies are spatially arranged. Note, however, that the band mobilities computed with the KG simulation scheme display a mathematical divergence (see Supporting Information, Figure S3 for details) in the band gap when $E \simeq 0$. This is because the mobility is inversely proportional to the number of charge carriers (n) (see eq 5) and the number of charges carriers vanishes when approaching the Fermi energy reference ($E_F{}^0$) corresponding to zero gate voltage (which was set at $E = 0$ eV here).

To shed light on the variation of the diffusion coefficient when sulfur vacancies are spatially arranged, we evaluate the one electron wave function (EWF) propagation in the MoS_2 monolayer as a function of time. EWF, as reported in Figure 5, is evaluated for the pristine MoS_2 monolayer as well as for the monolayer with one sulfur vacancy and also with twenty five sulfur vacancies that are randomly arranged. In the pristine case, the wave packet spreads through the material, unhindered, whereas the presence of sulfur vacancy scatters the wave packet, as can be seen in the case of one sulfur vacancy from Figure 5b. However, the presence of more sulfur vacancies can allow the formation of percolation pathways permitting spread of the wave packet, as demonstrated in Figure 5c. While scattering diminishes the ballistic diffusivity of the wave packet leading to a plateau represented by the semiclassical asymptotic limit of diffusivity (D_{max}), the formation of percolation pathways can enhance the absolute values of D_{max}. The difference in band mobilities in the MoS_2 monolayer when comparing the random sulfur vacancies (rD_1 and rD_2) to those of the spatially arranged sulfur vacancies (sD_1) can therefore be traced back to the spread of the wave packet as a function of time and the formation of percolation channels that can enhance charge carrier mobilities at any given vacancy concentration.

Sulfur Vacancies: Impact of Vacancy Concentration. As demonstrated in the previous section, the diffusion coefficient and the band mobilities of MoS_2 are not influenced by the presence of random sulfur vacancies either on one side or on both sides (rD_1 and rD_2) of the monolayer. Hereafter, the charge transport characteristics of the MoS_2 monolayer are therefore discussed as a function of different concentrations of

https://dx.doi.org/10.1021/acs.jpcc.0c04203
J. Phys. Chem. C 2020, 124, 15076−15084

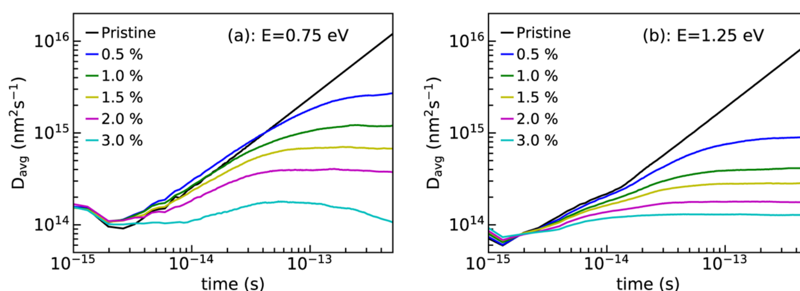

Figure 6. Diffusion coefficient of the MoS_2 monolayer for different concentrations of sulfur vacancies (up to 3%), obtained at (a) left: 0.75 eV in the conduction band and (b) right: 1.25 eV in the conduction band.

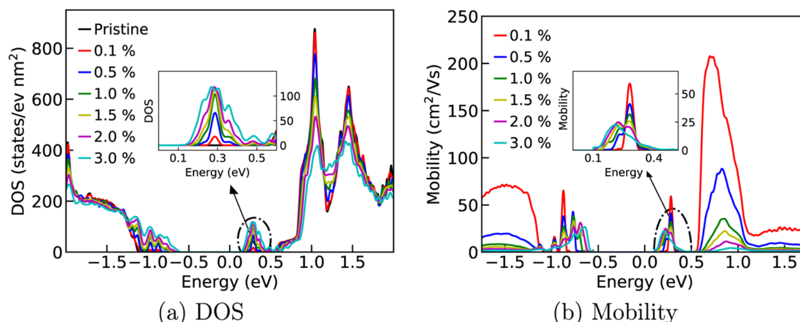

Figure 7. Calculated DOS and band mobility of the MoS_2 monolayer for different concentrations of sulfur vacancies (upto 3%). The mathematical divergence when $E \simeq 0$ is removed from the mobility plots for clarity.

randomly arranged sulfur vacancies, ranging from 0.1 to 3%, created on both sides of the monolayer. The diffusion coefficient, DOS, and band mobilities of MoS_2 as a function of vacancy concentration are reported in Figures 6 and 7. Calculations performed on larger 128 × 192 supercell of the pristine and defective MoS_2 monolayers, with size of 70.47 × 61.03 nm along the armchair and zigzag directions, show identical results (see Figure S2 for details).

With the increase in vacancy concentration, the mean diffusion coefficient in the semiclassical asymptotic limit (D_{max}) decreases as reported in Figure 6, and additional defect states start to evolve in the band gap, as presented in Figure 7a. This decrease in D_{max} with increase in vacancy concentration, in turn, leads to a decrease in band mobilities in the conduction band (Figure 7b), with highest electron mobilities (at any specific concentration) recorded at the band energies of ≈0.75 eV (in the window of 0.5 and 1.0 eV). The presence of additional defect states in the band gap induces a variation in both conductivity (see Supporting Information, Figure S3) and band mobilities within the band gap. The diffusion coefficient at the additional/defect states at ≈ 0.3 eV (see Supporting Information, Figure S4) in the band gap increases with the increase in sulfur vacancy concentration, contrary to D_{max} at ≈0.75 eV, as mentioned above. However, the diffusivity at these additional/defect states exhibits a localization regime (i.e., a weak localization phenomena), where an exponential decrease in the diffusivity is observed as a function of time, with a dependence on vacancy concentration. Therefore, the conductivities and band mobilities evaluated in this spectral region are to be taken with caution, as the quantum interferences and localization phenomena captured by the KG simulation scheme tend to vanish for experimental observations because of phonon scattering that destroys phase coherence, unless when observations at very low temperatures are invoked.

Having assessed the trend of charge transport characteristics of the MoS_2 monolayer as a function of sulfur vacancy concentration, we now turn our attention to the charge transport characteristics of charge carriers injected into the MoS_2 conduction band. As mentioned earlier, the field effect mobilities measured experimentally differ from the band mobilities, as demonstrated in refs 18 and 31. The band mobilities therefore need to be rescaled by using the density of charge carriers above (n_{loc}) and below the mobility edge (N_f) to obtain the calculated field effect mobilities, $\mu^F = \frac{N_f}{N_f + n_{loc}} \times \mu^B$.[31] The field effect mobilities (μ^F_{KG}) are therefore evaluated from the calculated KG band mobilities (μ^B_{KG}) at E = 0.75 eV, that is, close to the conduction band edge and with N_f set to 1.5×10^{13} cm^{-2} taken from ref 31. Our results are compared to the experimental data in Figure 8. The band and field effect mobilities evaluated in this work (μ^B_{KG} and

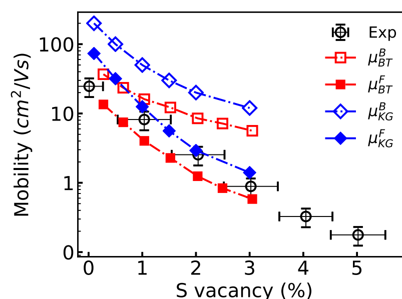

Figure 8. Comparison to the previous work of Bertolazzi *et al.*[31] The subscripts BT and KG represents the band (superscript: B) and field effect (superscript: F) mobilities, obtained using the scBTE (taken from ref 31 and the KG band mobilities, respectively. μ^B_{KG} is the maximum mobility of the MoS_2 monolayer obtained at band energies of 0.75 eV.

https://dx.doi.org/10.1021/acs.jpcc.0c04203
J. Phys. Chem. C 2020, 124, 15076−15084

μ_{KG}^{F}, respectively) show a power-law dependence as a function of sulfur vacancy concentration ($\mu \propto V_{S(\%)}^{-\gamma}$, γ being the falloff parameter), with a decrease of mobility at increased vacancy concentrations. These mobility trends are in close quantitative agreement with the experimental data, as well as with the band and field effect mobilities calculated with the scBTE scheme (μ_{BT}^{B} and μ_{BT}^{F}, respectively), reported by Bertolazzi *et al.*[31] The KG mobility trends (μ_{KG}^{F}) as well as those obtained earlier using the semi-classical Boltzmann transport scheme (μ_{BT}^{F}), where the scattering by charged impurities (vacancies) is included in a phenomenological way,[31] signify that the modulation of charge transport characteristics in MoS_2 monolayers is mainly because of the scattering of charge carriers at the sulfur vacancies.

CONCLUSIONS

oTB parameters of the sp^3d^5 form are reported for the MoS_2 monolayer (in its pristine and defect forms: sulfur vacancy) which are in good agreement with the reference DFT calculations in terms of their electronic band structures. These parameters are incorporated into the KG simulation scheme to compute the band and field effect mobilities. The electron mobilities from the charge carriers injected into the MoS_2 conduction band show a decrease in theoretical mobilities at increased vacancy concentrations that are in close quantitative agreement with the experimental data. It evolves that the sulfur vacancies act as scattering centers that modulate the charge transport characteristics in MoS_2 monolayers. Also, in comparison to random sulfur vacancies, spatially arranged sulfur vacancies at the same concentration can increase the mobility in MoS_2 monolayers because of the formation of percolation pathways permitting spread of the wavepacket. The experimental/theoretical formation of such vacancy clusters, however, needs further investigations. Also, the impact of interacting metal/chalcogen vacancies on the charge transport characteristics of MoS_2 monolayers as well as in other TMDC materials, needs the development of the additional tight-binding parameters, for which oTB parameters developed in this work can be used as a starting point.

ASSOCIATED CONTENT

Supporting Information

The Supporting Information is available free of charge at https://pubs.acs.org/doi/10.1021/acs.jpcc.0c04203.

> Orthogonal tight-binding (oTB) parameters, TB versus DFT band structure fit employed to derive the oTB parameters, diffusion coefficient of MoS_2 supercells replicated 128 × 192 times, along with the conductivity and mobility plots (PDF)

AUTHOR INFORMATION

Corresponding Authors

Sai Manoj Gali — *Laboratory for Chemistry of Novel Materials, University of Mons, 7000 Mons, Belgium;* orcid.org/0000-0002-0388-7888; Email: saimanoj.gali@umons.ac.be

David Beljonne — *Laboratory for Chemistry of Novel Materials, University of Mons, 7000 Mons, Belgium;* orcid.org/0000-0002-2989-3557; Email: david.beljonne@umons.ac.be

Authors

Anton Pershin — *Laboratory for Chemistry of Novel Materials, University of Mons, 7000 Mons, Belgium; Wigner Research Centre for Physics, H-1525 Budapest, Hungary*

Aurélien Lherbier — *Institute of Condensed Matter and Nanosciences, Université catholique de Louvain (UCLouvain), 1348 Louvain-la-Neuve, Belgium*

Jean-Christophe Charlier — *Institute of Condensed Matter and Nanosciences, Université catholique de Louvain (UCLouvain), 1348 Louvain-la-Neuve, Belgium*

Complete contact information is available at: https://pubs.acs.org/10.1021/acs.jpcc.0c04203

Notes

The authors declare no competing financial interest.

ACKNOWLEDGMENTS

This work was supported by the F.R.S.-FNRS through the "TOREADOR" project (T.0051.18), the Fédération Wallonie-Bruxelles through the Action de Recherche Concertée (ARC) on "3D nanoarchitecturing of 2D crystals" (no. 16/21-077), the European Union's Horizon 2020 research and innovation program (GrapheneFlagship Core1-no. 696656 and Core2-no. 785219). DB is the FNRS Research Director. A.L. and J.-C.C. acknowledge the Francqui-Stichting Foundation and the Fonds de la Recherche Scientifique de Belgique. A.P. acknowledges the support from EU H2020 Quantum Technology Flagship project ASTERIQS (grant no. 820394). Computational resources were provided by the supercomputing facilities of the Consortium des Équipements de Calcul Intensif en Fédération Wallonie Bruxelles (CÉCI) funded by the F.R.S.-FNRS under the convention no. 2.4.617.07.F and no. 2.5020.11.

REFERENCES

(1) Geim, A. K.; Grigorieva, I. V. Van der Waals heterostructures. *Nature* **2013**, *499*, 419−425.

(2) Butler, S. Z.; et al. Progress, challenges and opportunities in two-dimensional materials beyond graphene. *ACS Nano* **2013**, *7*, 2898−2926.

(3) Geim, A. K. Graphene: Status and Prospects. *Science* **2009**, *324*, 1530−1534.

(4) Castro Neto, A. H.; Guinea, F.; Peres, N. M. R.; Novoselov, K. S.; Geim, A. K. The electronic properties of graphene. *Rev. Mod. Phys.* **2009**, *81*, 109−162.

(5) Mas-Ballesté, R.; Gómez-Navarro, C.; Gómez-Herrero, J.; Zamora, F. 2D materials: to graphene and beyond. *Nanoscale* **2011**, *3*, 20−30.

(6) Zhang, X.; Hou, L.; Ciesielski, A.; Samorì, P. 2D Materials beyond rraphene for high-performance energy storage applications. *Adv. Energy Mater.* **2016**, *6*, 1600671.

(7) Van Le, Q.; Choi, J.-Y.; Kim, S. Y. Recent advances in the application of two-dimensional materials as charge transport layers in organic and perovskite solar cells. *FlatChem* **2017**, *2*, 54−66.

(8) Karahan, H. E.; Wang, Y.; Li, W.; Liu, F.; Wang, L.; Sui, X.; Riaz, M. A.; Chen, Y. Antimicrobial graphene materials: the interplay of complex materials characteristics and competing mechanisms. *Biomater. Sci.* **2018**, *6*, 766−773.

(9) Bhimanapati, G. R.; et al. Recent advances in two-dimensional materials beyond Graphene. *ACS Nano* **2015**, *9*, 11509−11539.

(10) Fiori, G.; Bonaccorso, F.; Iannaccone, G.; Palacios, T.; Neumaier, D.; Seabaugh, A.; Banerjee, S. K.; Colombo, L. Electronics based on two-dimensional materials. *Nat. Nanotechnol.* **2014**, *9*, 768.

(11) Yazyev, O. V.; Kis, A. MoS2 and semiconductors in the flatland. *Mater. Today* **2015**, *18*, 20−30.

(12) Radisavljevic, B.; Radenovic, A.; Brivio, J.; Giacometti, V.; Kis, A. Single-layer MoS2 transistors. *Nat. Nanotechnol.* **2011**, *6*, 147.
(13) Lembke, D.; Bertolazzi, S.; Kis, A. Single-layer MoS2 electronics. *Acc. Chem. Res.* **2015**, *48*, 100−110.
(14) Li, X.; Mullen, J. T.; Jin, Z.; Borysenko, K. M.; Buongiorno Nardelli, M.; Kim, K. W. Intrinsic electrical transport properties of monolayer silicene and MoS_2 from first principles. *Phys. Rev. B: Condens. Matter Mater. Phys.* **2013**, *87*, 115418.
(15) Li, W. Electrical transport limited by electron-phonon coupling from Boltzmann transport equation: An ab initio study of Si, Al, and MoS_2. *Phys. Rev. B: Condens. Matter Mater. Phys.* **2015**, *92*, 075405.
(16) Kaasbjerg, K.; Thygesen, K. S.; Jacobsen, K. W. Phonon-limited mobility in n-type single-layer MoS_2 from first principles. *Phys. Rev. B: Condens. Matter Mater. Phys.* **2012**, *85*, 115317.
(17) Yu, Z.; Zhun-Yong, O.; Pan, Y.; Cui, Y.; Xin, R.; Shi, Y.; Wang, B.; Wu, Y.; Chen, T.; Zhang, Y.-W.; Zhang, G.; Wang, X. Realization of room-temperature phonon-limited carrier transport in monolayer MoS2 by dielectric and carrier screening. *Adv. Mater.* **2015**, *28*, 547−552.
(18) Zhu, W.; Low, T.; Lee, Y.-H.; Wang, H.; Farmer, D. B.; Kong, J.; Xia, F.; Avouris, P. Electronic transport and device prospects of monolayer molybdenum disulphide grown by chemical vapour deposition. *Nat. Commun.* **2014**, *5*, 3087.
(19) Najmaei, S.; Liu, Z.; Zhou, W.; Zou, X.; Shi, G.; Lei, S.; Yakobson, B. I.; Idrobo, J.-C.; Ajayan, P. M.; Lou, J. Vapour phase growth and grain boundary structure of molybdenum disulphide atomic layers. *Nat. Mater.* **2013**, *12*, 754−759.
(20) Zhou, W.; Zou, X.; Najmaei, S.; Liu, Z.; Shi, Y.; Kong, J.; Lou, J.; Ajayan, P. M.; Yakobson, B. I.; Idrobo, J.-C. Intrinsic Structural Defects in Monolayer Molybdenum Disulfide. *Nano Lett.* **2013**, *13*, 2615−2622.
(21) Yu, Z. G.; Zhang, Y.-W.; Yakobson, B. I. An anomalous formation pathway for dislocation-sulfur vacancy complexes in polycrystalline monolayer MoS2. *Nano Lett.* **2015**, *15*, 6855−6861.
(22) Liu, D.; Guo, Y.; Fang, L.; Robertson, J. Sulfur vacancies in monolayer MoS2 and its electrical contacts. *Appl. Phys. Lett.* **2013**, *103*, 183113.
(23) Wang, L.; et al. Artificial synapses based on multiterminal memtransistors for neuromorphic application. *Adv. Funct. Mater.* **2019**, *29*, 1901106.
(24) Komsa, H.-P.; Kotakoski, J.; Kurasch, S.; Lehtinen, O.; Kaiser, U.; Krasheninnikov, A. V. Two-dimensional transition metal dichalcogenides under electron irradiation: defect production and doping. *Phys. Rev. Lett.* **2012**, *109*, 035503.
(25) Hong, J.; et al. Exploring atomic defects in molybdenum disulphide monolayers. *Nat. Commun.* **2015**, *6*, 6293.
(26) Roy, S.; Choi, W.; Jeon, S.; Kim, D.-H.; Kim, H.; Yun, S. J.; Lee, Y.; Lee, J.; Kim, Y.-M.; Kim, J. Atomic observation of filling vacancies in monolayer transition metal sulfides by chemically sourced sulfur atoms. *Nano Lett.* **2018**, *18*, 4523−4530.
(27) Yu, Z.; Pan, Y.; Shen, Y.; Wang, Z.; Ong, Z.-Y.; Xu, T.; Xin, R.; Pan, L.; Wang, B.; Sun, L.; Wang, J.; Zhang, G.; Zhang, Y. W.; Shi, Y.; Wang, X. Towards intrinsic charge transport in monolayer molybdenum disulfide by defect and interface engineering. *Nat. Commun.* **2014**, *5*, 5290.
(28) KC, S.; Longo, R. C.; Addou, R.; Wallace, R. M.; Cho, K. Impact of intrinsic atomic defects on the electronic structure of MoS2 monolayers. *Nanotechnology* **2014**, *25*, 375703.
(29) Zhou, W.; Zou, X.; Najmaei, S.; Liu, Z.; Shi, Y.; Kong, J.; Lou, J.; Ajayan, P. M.; Yakobson, B. I.; Idrobo, J.-C. Intrinsic structural defects in monolayer molybdenum disulfide. *Nano Lett.* **2013**, *13*, 2615−2622.
(30) Sim, D. M.; Kim, M.; Yim, S.; Choi, M.-J.; Choi, J.; Yoo, S.; Jung, Y. S. Controlled doping of vacancy-containing few-layer MoS2 via highly stable thiol-based molecular chemisorption. *ACS Nano* **2015**, *9*, 12115−12123.
(31) Bertolazzi, S.; Bonacchi, S.; Nan, G.; Pershin, A.; Beljonne, D.; Samori, P. Engineering chemically active defects in monolayer MoS2 transistors via ion-beam irradiation and their healing via vapor deposition of alkanethiols. *Adv. Mater.* **2017**, *29*, 1606760.
(32) Leconte, N.; Lherbier, A.; Varchon, F.; Ordejon, P.; Roche, S.; Charlier, J.-C. Quantum transport in chemically modified two-dimensional graphene: From minimal conductivity to Anderson localization. *Phys. Rev. B: Condens. Matter Mater. Phys.* **2011**, *84*, 235420.
(33) de Laissardière, G. T.; Mayou, D. Conductivity of graphene with resonant and nonresonant adsorbates. *Phys. Rev. Lett.* **2013**, *111*, 146601.
(34) Gargiulo, F.; Autès, G.; Virk, N.; Barthel, S.; Rösner, M.; Toller, L. R. M.; Wehling, T. O.; Yazyev, O. V. Electronic transport in graphene with aggregated hydrogen adatoms. *Phys. Rev. Lett.* **2014**, *113*, 246601.
(35) Lherbier, A.; Dubois, S. M.-M.; Declerck, X.; Niquet, Y.-M.; Roche, S.; Charlier, J.-C. Transport properties of graphene containing structural defects. *Phys. Rev. B: Condens. Matter Mater. Phys.* **2012**, *86*, 075402.
(36) Radchenko, T. M.; Shylau, A. A.; Zozoulenko, I. V.; Ferreira, A. Effect of charged line defects on conductivity in graphene: Numerical Kubo and analytical Boltzmann approaches. *Phys. Rev. B: Condens. Matter Mater. Phys.* **2013**, *87*, 195448.
(37) Radchenko, T. M.; Tatarenko, V. A.; Sagalianov, I. Y.; Prylutskyy, Y. I. Effects of nitrogen-doping configurations with vacancies on conductivity in graphene. *Phys. Lett. A* **2014**, *378*, 2270−2274.
(38) Lherbier, A.; Blase, X.; Niquet, Y.-M.; Triozon, F.; Roche, S. Charge transport in chemically doped 2D graphene. *Phys. Rev. Lett.* **2008**, *101*, 036808.
(39) Lherbier, A.; Roche, S.; Restrepo, O. A.; Niquet, Y.-M.; Delcorte, A.; Charlier, J.-C. Highly defective graphene: A key prototype of two-dimensional Anderson insulators. *Nano Res.* **2013**, *6*, 326−334.
(40) Roldán, R.; López-Sancho, M. P.; Guinea, F.; Cappelluti, E.; Silva-Guillén, J. A.; Ordejón, P. Momentum dependence of spin−orbit interaction effects in single-layer and multi-layer transition metal dichalcogenides. *2D Materials* **2014**, *1*, 034003.
(41) Yuan, S.; Roldán, R.; Katsnelson, M. I.; Guinea, F. Effect of point defects on the optical and transport properties of MoS_2 and WS_2. *Phys. Rev. B: Condens. Matter Mater. Phys.* **2014**, *90*, 041402.
(42) Zahid, F.; Lei, L.; Yu, Z.; Jian, W.; Hong, G. A generic tight-binding model for monolayer, bilayer and bulk MoS2. *AIP Adv.* **2013**, *3*, 052111.
(43) Lian, J. X.; Lherbier, A.; Wang, L. J.; Charlier, J.-C.; Beljonne, D.; Olivier, Y. Electronic structure and charge transport in nanostripped graphene. *J. Phys. Chem. C* **2016**, *120*, 20024−20032.
(44) Tonnelé, C.; Pershin, A.; Gali, S. M.; Lherbier, A.; Charlier, J.-C.; Castet, F.; Muccioli, L.; Beljonne, D. Atomistic simulations of charge transport in photoswitchable organic-graphene hybrids. *JPhys Mater.* **2019**, *2*, 035001.
(45) Giannozzi, P.; et al. QUANTUM ESPRESSO: a modular and open-source software project for quantum simulations of materials. *J. Phys. Condens. Matter* **2009**, *21*, 395502.
(46) Kadantsev, E. S.; Hawrylak, P. Electronic structure of a single MoS2 monolayer. *Solid State Commun.* **2012**, *152*, 909−913.
(47) Slassi, A.; Cornil, J. Theoretical characterization of strain and interfacial electronic effects in donor-acceptor bilayers of 2D transition metal dichalcogenides. *2D Materials* **2018**, *6*, 015025.
(48) Qiu, H.; Xu, T.; Wang, Z.; Ren, W.; Nan, H.; Ni, Z.; Chen, Q.; Yuan, S.; Miao, F.; Song, F.; Long, G.; Shi, Y.; Sun, L.; Wang, J.; Wang, X. Hopping transport through defect-induced localized states in molybdenum disulphide. *Nat. Commun.* **2013**, *4*, 3642.
(49) Triozon, F.; Vidal, J.; Mosseri, R.; Mayou, D. Quantum dynamics in two- and three-dimensional quasiperiodic tilings. *Phys. Rev. B: Condens. Matter Mater. Phys.* **2002**, *65*, 220202.
(50) Ishii, H.; Triozon, F.; Kobayashi, N.; Hirose, K.; Roche, S. Charge transport in carbon nanotubes based materials: a Kubo−Greenwood computational approach. *C. R. Phys.* **2009**, *10*, 283−296.

(51) Parkin, W. M.; Balan, A.; Liang, L.; Das, P. M.; Lamparski, M.; Naylor, C. H.; Rodríguez-Manzo, J. A.; Johnson, A. T. C.; Meunier, V.; Drndić, M. Raman shifts in electron-irradiated monolayer MoS2. *ACS Nano* **2016**, *10*, 4134−4142.
(52) Vancsó, P.; Magda, G. Z.; Pető, J.; Noh, J.-Y.; Kim, Y.-S.; Hwang, C.; Biró, L. P.; Tapasztó, L. The intrinsic defect structure of exfoliated MoS2 single layers revealed by Scanning Tunneling Microscopy. *Sci. Rep.* **2016**, *6*, 26726.
(53) Komsa, H.-P.; Kurasch, S.; Lehtinen, O.; Kaiser, U.; Krasheninnikov, A. V. From point to extended defects in two-dimensional MoS_2: Evolution of atomic structure under electron irradiation. *Phys. Rev. B: Condens. Matter Mater. Phys.* **2013**, *88*, 035301.
(54) Le, D.; Rawal, T. B.; Rahman, T. S. Single-Layer MoS2 with sulfur vacancies: structure and catalytic application. *J. Phys. Chem. C* **2014**, *118*, 5346−5351.
(55) Zhou, S.; Wang, S.; Li, H.; Xu, W.; Gong, C.; Grossman, J. C.; Warner, J. H. Atomic structure and dynamics of defects in 2D MoS2 bilayers. *ACS Omega* **2017**, *2*, 3315−3324.

https://dx.doi.org/10.1021/acs.jpcc.0c04203
J. Phys. Chem. C 2020, 124, 15076−15084